Collection Efficiency of Nanosize Particles in a Two-Stage Electrostatic Precipitator

Mingheng Li and Panagiotis D. Christofides*

Department of Chemical and Biomolecular Engineering, University of California, Los Angeles, California 90095-1592

The collection efficiency of particles in the nanosize range (5−100 nm) in a two stage parallel plate electrostatic precipitator is studied by numerical simulation based on a fundamental model of the process. Specifically, the particle charging process is based on Fuchs' theory. For the collecting stage, the model employs an Eulerian approach for the solid−gas flow and explicitly accounts for Brownian and eddy diffusion, turbulent flow, and electrostatic migration. Calculation results indicate that particles in the nanosize range are not uniformly charged. Ultrafine particles with diameter less than 20 nm seldom acquire more than one unit of elementary charge. Larger particles (20−100 nm) may carry several units of charge, depending on the product of ion concentration and charging time. The simulation results also indicate that there is a local maximum in the collection efficiency in the nanosize range, a finding which is consistent with experimental observations reported in the literature. The simulation also points out that the most efficient way to increase the collection efficiency of particles in the ultrafine size range is to enhance the charging process. For particles with larger size, both the parameters in the charging stage (the product of ion concentration and charging time) and those in the collecting stage (electrostatic intensity and length and width of the collecting cell) have an important effect on the overall collection efficiency.

1. Introduction

The environmental pollution has become, during the recent years, a crucial problem of public concern, and the authorities are requested to set increasingly more stringent limits for the emissions from the industrial plants for solid particulate and other gaseous pollutants. The electrostatic precipitator, as a consequence, has become one of the most commonly employed particulate control devices for collecting aerosols from utility boilers, incinerators, and many other industrial processes.[1] Furthermore, with the development of sophisticated nanoparticle synthesis techniques, the electrostatic precipitator also provides a powerful tool for collecting nanoparticles from an aerosol or plasma reactor.[2−4] The greatest advantage provided by an electrostatic precipitator is that the electrostatic force of highly charged particles under the influence of an external electrostatic field is usually very large, as compared to gravitational, thermal, and inertial forces. The electrostatic precipitation involves two major physical processes: particle charging in an electric field and turbulent transport of charged particles to the collection surface under the electrostatic field. For coarse particles (larger than 100 nm), experimental work has shown that the collection efficiency is very high (usually larger than 99%).[5] For particles with diameter less than 100 nm, however, only moderate collection efficiency can be achieved, which might be explained by the low charging fraction of nanosize particles.[6] A fundamental understanding, with the aid of numerical simulation, will shed light onto the behavior of this process and help to improve its design and operation.

Figure 1 shows a schematic of a typical two-stage plate electrostatic precipitator. In the charging stage, high voltage is applied to a wire to generate a corona discharge and the particles suspended in the air are electrically charged as they are exposed in the unipolar ions. In the collection stage, high voltage is applied in the middle of two grounded plates. When the air moves through the collection channel, the suspended particles migrate to the grounded plates as a result of the electrostatic forces. Two fundamental models (i.e., laminar and Deutsch models) are usually applied to estimate the collection efficiency of particles in an electrostatic precipitator. Although both models make the assumption of plug flow (i.e., the velocity profile is flat as the gas moves forward), they treat differently the turbulent dispersion of particles in the gas field. In the Deutsch model the transverse turbulent dispersion is considered to be infinite so that there is no gradient of particle concentration across the precipitator duct. As a result, the mass flux normal to the collecting plates is proportional to the longitudinal concentration gradient and the particle concentration decays exponentially in the flow direction. In the so-called "laminar" model, however, the transverse turbulent dispersion is negligible, and the mass flux to the collecting plates is uniform. Consequently, the particle concentration decays as a linear function of the longitudinal coordinate. Referring to Figure 1, if one let $De = c_e L/(Ru_0)$ be the Deutsch number, where c_e is the particle migration velocity normal to the collecting plate, u_0 is the average longitudinal velocity, and L and R are the length and half width of each collection cell in the electrostatic precipitator, the collection efficiency in the above two cases can be described as follows:

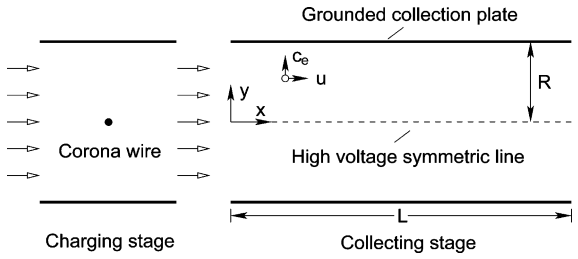

Figure 1. Schematic diagram of a typical two-stage electrostatic precipitator.

* To whom correspondence should be addressed. Tel.: (310) 794-1015. Fax: (310) 206-4107. E-mail: pdc@seas.ucla.edu.

10.1021/ie060101r CCC: $33.50
Published on Web 04/12/2006

$$\eta = \begin{cases} 1 - \exp(-De) & \text{(Deutsch model)} \\ \min\{De, 1\} & \text{(Laminar model)} \end{cases} \quad (1)$$

When the diffusivity is finite, the collection efficiency will be bounded by the one predicted by laminar and Deutsch models. Leonard et al.[7] introduced a finite and uniformly distributed particle diffusivity into the governing transport equation and obtained an analytical solution to the collection efficiency as a function of both the Deutsch number and the Peclet number ($Pe = c_e R/D_p$, where D_p is the particle diffusivity). When the diffusivity is close to zero (or $Pe \rightarrow \infty$), the collection efficiency tends to the one predicted by the laminar model, while for infinite diffusivity (or $Pe \rightarrow 0$), the collection efficiency approaches the one predicted by the Deutsch model. However, the assumption of uniform diffusivity is not adequate to describe the particle transport phenomena near the wall, where the diffusivity is significantly smaller than the one in the turbulent core. More realistic assumptions toward the nonuniform distribution of particle diffusivity were made in subsequent research work. For example, the flow field was divided into two zones and the particle diffusivity was taken to increase as a linear function of its distance from the collecting wall in the boundary layer region and become constant in the core region.[8−10] Moreover, because the flow field is not usually uniformly distributed, the plug flow assumption also needs to be modified.[10−12] In this sense, it is more reasonable to take into account the spatially distributed diffusivity and velocity. With the development of more advanced computational technologies and facilities, the collection efficiency of particles in an electrostatic precipitator was successfully simulated and analyzed by state of the art computational fluid dynamics,[13] direct numerical simulations,[14,15] and Monte Carlo simulations.[12,16] The collection efficiency of polydisperse particles using the method of moments was also reported.[17,18] The reader may refer to the work of Varonos et al.[19] for a discussion of the various optimization issues of electrostatic precipitation processes.

Despite a plethora of analytical and numerical work on the electrostatic precipitation process in the literature, the behavior of nanosize particles in an electrostatic precipitator has been rarely discussed. Different from coarse particles, particles in the nanosize range are not uniformly charged even if they are monodisperse. Because the collection efficiency is not a linear function of the number of charges carried by a particle, prediction of the overall collection efficiency of monodisperse particles in the nanosize range should take into account the charging distribution instead of using an average charging level. In this paper, important issues of nanosize particles in electrostatic precipitation, such as unipolar charging, turbulent deposition of charged particles under the electrostatic field, and overall collection efficiency of particles accounting for charging distribution in an electrostatic precipitator, are presented and analyzed numerically. By exploring the mechanism of the particle removal underlying the electrostatic precipitation process, we aim to provide a fundamental insight into this process and to point out several crucial factors that affect the overall collection efficiency.

2. Particle Charging Process

Attachment of small ions via either field charging or diffusion charging is one of the most commonly used mechanisms by which aerosol particles can be charged.[20] For particles falling in the submicrometer size range, the dominant mechanism is diffusion charging, which can be divided into three regimes based on the magnitude of the Knudsen number Kn ($Kn = 2\lambda_{ion}/d_p$, where λ_{ion} is the mean free path of ions, which is about 0.0145 μm under atmospheric pressure, and d_p is the particle diameter). In the continuum regime ($Kn \ll 1$), where the particle diameter is larger than 100 nm, the particle charging can be determined by solving the macroscopic diffusion equations. In the free molecule regime ($Kn \gg 1$), where the particle diameter is less than 10 nm, the theory of Marlow and Brock[21] best predicts the charging process. In the transition regime ($Kn \approx 1$), where the particle diameter is larger than 10 nm but less than 100 nm, approaches proposed by Fuchs[22] and Marlow and Brock work well.

For nanosize particles ($d_p = 5-100$ nm), the unipolar charging process is described by the following set of dynamic equations:[6,23,24]

$$\begin{aligned} \frac{dn_0}{dt} &= -\beta_0 n_{ion} n_0 \\ \frac{dn_1}{dt} &= \beta_0 n_{ion} n_0 - \beta_1 n_{ion} n_1 \\ &\vdots \\ \frac{dn_i}{dt} &= \beta_{i-1} n_{ion} n_{i-1} - \beta_i n_{ion} n_i \\ &\vdots \end{aligned} \quad (2)$$

where n_i is the concentration of particles carrying i units of charge and n_{ion} is the concentration of ions. The positive term at the right-hand side of each equation stands for the rate of increase in the particle concentration and the negative term stands for the rate of decrease. The combination coefficient β_i, which represents the valid collision rate of a particle carrying i units of charge with an ion is described by Fuchs' theory:[22]

$$\beta_i = \frac{\pi C_{ion} \xi \delta^2 \exp[-\phi(\delta)/kT]}{1 + \exp[-\phi(\delta)/kT] \frac{C_{ion} \xi \delta^2}{4 D_{ion} a} \int_0^{a/\delta} \exp[\phi(a/x)/kT]\, dx} \quad (3)$$

where k is the Boltzmann constant, T is the temperature, ϕ is the electrostatic potential between particles and ions, ξ is the probability of collisions, δ is the radius of the "limiting sphere", and D_{ion} and C_{ion} are the diffusion coefficient and mean thermal velocity of the ions, respectively. All the parameters appearing in eq 3 can be calculated by the following equations:[6,24,25]

$$\phi(r) = \frac{e^2}{4\pi\epsilon_0 r}\left[i - \frac{\kappa - 1}{\kappa + 1}\frac{a^3}{2r(r^2 - a^2)}\right]$$

$$\delta = \frac{a}{Kn^2}\left[\frac{1}{5}(1 + Kn)^5 - \frac{1}{3}(1 + Kn^2)(1 + Kn)^3 + \frac{2}{15}(1 + Kn^2)^{2.5}\right]$$

$$\xi = \max\left\langle \min\left\{ \frac{r_a^2}{\delta^2}\left(1 + \frac{2[\phi(\delta) - \phi(r_a)]}{3kT}\right)\right\}, 0\right\rangle$$

$$D_{\text{ion}} = \frac{kTZ_{\text{ion}}}{e}$$

$$C_{\text{ion}} = \sqrt{\frac{8kT}{\pi(M_{\text{ion}}/N_{\text{a}})}}$$

$$\lambda_{\text{ion}} = 1.329\frac{Z_{\text{ion}}}{e}\sqrt{\frac{kTM_{\text{ion}}M_{\text{air}}}{(M_{\text{ion}} + M_{\text{air}})N_{\text{a}}}} \tag{4}$$

where a is the radius of a particle, e is the elementary electrostatic charge, κ is the dielectric constant of a particle, and ϵ_0 is the dielectric constant of free space. Apparently, the combination coefficient varies with the size of the particle and the number of elementary charges it carries.

Let $\vec{n} = [n_0\ n_1\ ...\ n_p]^{\text{T}}$ be the concentration distribution of particles with different number of charges and p be the maximum number of charges a particle can carry (i.e., any β_i with $i \geq p$ is zero); the equations to describe the charging process can be rewritten in the following form:

$$\frac{\text{d}\vec{n}}{\text{d}t} = \mathbf{A}n_{\text{ion}}\vec{n} \tag{5}$$

where $\mathbf{A}$ is a matrix of the following form

$$\mathbf{A} = \begin{bmatrix} -\beta_0 & 0 & \cdots & \cdots & \cdots & 0 \\ \beta_0 & -\beta_1 & \ddots & & & \vdots \\ 0 & \beta_1 & -\beta_2 & \ddots & & \vdots \\ \vdots & \ddots & \ddots & \ddots & \ddots & \vdots \\ \vdots & & \ddots & \beta_{p-2} & -\beta_{p-1} & 0 \\ 0 & \cdots & \cdots & 0 & \beta_{p-1} & 0 \end{bmatrix} \tag{6}$$

The solution to eq 5 is given by

$$\vec{n}(t) = \exp(\mathbf{A}n_{\text{ion}}t)\vec{n}_0 \tag{7}$$

where $\exp(\mathbf{A}n_{\text{ion}}t)$ is a matrix the same size as $\mathbf{A}$ and $\vec{n}_0 = [n_{\text{T}}0\ ...\ 0]^{\text{T}}$ (where n_{T} is the initial concentration of particles without charge). There are many ways to calculate the exponential of matrix $\mathbf{A}n_{\text{ion}}t$. Referring to eq 6, one can easily find out that the matrix $\mathbf{A}$ has $p + 1$ distinct eigenvalues $-\beta_0 < -\beta_1 < ... < -\beta_{p-1} < 0$, and it can be diagonalized as $\mathbf{A} = P\Lambda P^{-1}$, where $\Lambda = \text{diag}[-\beta_0\ -\beta_1\ ...\ -\beta_{p-1}\ 0]$ and both P and P^{-1} are lower triangular matrixes that can be determined analytically. According to linear systems theory,[26] we have

$$\vec{n}(t) = P\ \text{diag}[\exp(-\beta_0 n_{\text{ion}}t)\ \exp(-\beta_1 n_{\text{ion}}t)\ ...\ \exp(-\beta_{p-1}n_{\text{ion}}t)\ 1]P^{-1}\vec{n}_0 \tag{8}$$

When the product $(n_{\text{ion}}t)$ goes to infinity, the particle charging will be saturated, and its charge distribution is given by

$$\lim_{n_{\text{ion}}t\to\infty} \vec{n}(t) = P\ \text{diag}[0\ 0\ ...\ 0\ 1]P^{-1}\vec{n}_0 = [0\ 0\ ...\ 0\ n_{\text{T}}]^{\text{T}} \tag{9}$$

which implies that the particles will all be charged by p units of charge after saturation.

Another method to compute the exponential of the matrix $\mathbf{A}n_{ion}t$ is to apply Taylor's expansion and to truncate the high order terms whose norms are sufficiently small. In this work, eq 7 is solved directly using the command "*expm*" in the Matlab software package, which is based on a scaling and squaring algorithm with a Pade approximation. Theoretically, the dimension of the matrix $\mathbf{A}$ is infinity. However, as will be shown later, as a result of the sharp decay of β, the highest number of elementary charges a nanosize particle can carry is very small (generally less than 10 under the operating conditions of interest in this work). Therefore, the dimension of matrix $\mathbf{A}$ is small. In the numerical calculation, the optimal dimension of $\mathbf{A}$ $(=p + 1)$ is chosen such that a further increase of p has no effect on the charging distribution.

3. Particle Collection Process

The mass transport behavior of nanosize particles in a two-stage parallel electrostatic precipitator is explored by numerical simulations in this work. Generally speaking, the gas−solid flow can be described in two ways, namely, the Lagrangian and the Eulerian methods. In the Lagrangian approach, the gas phase is treated as a continuum and the trajectory of each individual particle is solved by momentum transfer equations.[12−15,27] In the Eulerian approach, however, the continuum hypothesis is made for both the particulate phase and the gas phase.[10,11,17,25,28,29] In this paper, we employed the Eulerian approach to calculate the distribution of the particle concentration. The readers may refer to our previous work for the modeling and control of a variety of particulate processes.[30−35] Under the assumptions of (1) steady state, (2) negligible axial diffusion, and (3) insignificant gravitational force, the particle transport equation in the electrostatic precipitator and its corresponding boundary conditions can be written as follows:

$$\frac{\partial(un)}{\partial x} + \frac{\partial(c_{\text{e}}n)}{\partial y} = \frac{\partial}{\partial y}\left(D_{\text{p}}\frac{\partial n}{\partial y}\right)$$

B.C.

$$n = n_0, \quad \forall y, \quad x = 0$$

$$n = 0, \quad \forall x, \quad y = R$$

$$-D_p\frac{\partial n}{\partial y} + c_{\text{e}}n = 0, \quad \forall x, \quad y = 0 \tag{10}$$

where n is the particle concentration, u is the longitudinal velocity, c_{e} is the migration velocity along the y direction, determined by $c_{\text{e}} = [ieE/(3\pi\mu d_{\text{p}})]C$, and $D_{\text{p}} = D_{\text{b}} + \epsilon$. In the previous equations, D_{b} is the Brownian diffusivity determined by the Stokes−Einstein equation $D_{\text{b}} = [kT/(3\pi\mu d_{\text{p}})]C$, ϵ is the turbulent diffusivity, and C is the slip factor which can be calculated by $C = 1 + Kn[1.257 + 0.4\ \exp(-1.1/Kn)]$.[1]

As for the boundary conditions, it is assumed that the collecting plates behave as an ideal perfect sink and the particle concentration is zero. This assumption was justified by Park and Chun.[10] Note that the assumption of zero concentration gradient at the collecting wall was also made in other references.[7,17,36] At the symmetric surface $(y = 0)$, a zero net flux is assumed such that there is no accumulation of mass at the symmetric surface, that is, the flux caused by the turbulent dispersion cancels the one by electrostatic migration. The particle wall interaction is not included in this work. The re-entrainment effect can be taken into account by modifying the boundary conditions.[8]

To account for the transverse particle velocity distribution, we applied the well-known "law of the wall" relationships in

the viscous sublayer, the buffer region, the constant-stress layer (logarithmic region), and the "power-law" region[37] (pp 615−638). We also changed the constant 4.9 to 5.0 for the velocity relationship in the logarithmic distribution region to make it smoother. Specifically,

$$u^+ = \begin{cases} y^+, y^+ < 5 \\ 2.5\ln(1+0.4y^+) + 7.4[1-\exp(-y^+/11) - \\ \qquad \exp(-0.33y^+)y^+/11],\ 5 \le y^+ < 30 \\ 2.44\ln(y^+) + 5.0,\ 30 \le y^+ < 500 \\ 8.3(y^+)^{1/7},\ y^+ \ge 500 \end{cases} \quad (11)$$

where u^+ and the y^+ are the dimensionless velocity and distance defined by $u^+ = u/u^*$ and $y^+ = y'u^*/\nu$. Note $y' = R - y$ because of the different coordinates. The other parameters are related by $u^* = (\tau_w/\rho)^{1/2}$, $f = 4\tau_w/(^1/_2\rho_f u_0^2)$, $1/\sqrt{f} = 2.0\log(\sqrt{f}Re_{D_h}) - 0.8$, and Re_{D_h} is defined based on the hydraulic diameter.[10,17]

The turbulent dispersion coefficient was assumed to be uniform in the turbulent core of the flow and decay to zero at the collection plate wall following a linear function, which was used in the literacture.[9,10] Specifically, it takes the following form

$$\epsilon = \begin{cases} 10\epsilon_0 y'/R,\ 0 \le y' \le 0.1R \\ \epsilon_0,\ 0.1R < y' \le R \end{cases} \quad (12)$$

where ϵ_0 is the turbulent dispersion coefficient within the turbulent core of the flow which is estimated by[9,10]

$$\epsilon_0 = 0.04u^*R \quad (13)$$

Implementation of the expressions of spatially distributed particle velocity (eq 11) and diffusivity (eqs 12 and 13) into the particle transport equation (eq 10) yields

$$u\frac{\partial n}{\partial x} + a\frac{\partial n}{\partial y} = b\frac{\partial^2 n}{\partial^2 y} \quad (14)$$

where $a = c_e + 10\epsilon_0/R$ and $b = D_b + 10\epsilon_0(R - y)/R$ if $y' \le 0.1R$ and $a = c_e$ and $b = D_b + \epsilon_0$ if $y' > 0.1R$.

Using the upwind finite difference scheme, the particle concentration at each grid point in the electrostatic precipitator can be calculated by the following iterative formulas

$$n_j^{i+1} = \begin{cases} (\alpha+\beta)n_{j-1}^{\ i} + (1-\alpha-2\beta)n_j^{\ i} + \beta n_{j+1}^{\ i}\ (\text{if } \alpha > 0) \\ \beta n_{j-1}^{\ i} + (1+\alpha-2\beta)n_j^{\ i} + (\beta-\alpha)n_j{+}1^{i}\ (\text{if } \alpha \le 0) \end{cases}$$

for $i = 1, ..., M$ and $j = 2, ..., K$

$$n_1^{\ i} = \frac{D_p}{D_p + c_e\Delta y}n_2^{\ i},\quad \text{for } i = 2, 3, ..., M+1$$

$$n_{K+1}^{\ i} = 0,\quad \text{for } i = 2, 3, ..., M+1$$

$$n_j^{\ 1} = n_0,\quad \text{for } j = 1, 2, ..., K+1 \quad (15)$$

where $\alpha(y) = a\Delta x/(u\Delta y)$, $\beta(y) = b\Delta x/(u\Delta^2 y)$, and $M + 1$ and $K + 1$ are the total number of nodes along x and y directions, respectively.

The collection efficiency of particles having i units of charge is given by the following formula:

$$\eta_i = 1 - \frac{\int_0^R u(x,y)\, n(x,y)|_{x=L}\, dy}{\int_0^R u(x,y)\, n(x,y)|_{x=0}\, dy} \quad (16)$$

which is calculated numerically. The overall collection efficiency (η_t) is determined as the weighted sum of each single collection efficiency of the particles having different numbers of charges:

$$\eta_t = \sum_{i=0}^{\infty}\eta_i f_i \quad (17)$$

where f_i is the fraction of particles having i units of charge. Although the collection efficiency based on the average number of charges (usually nonintegers) might be used, we believe that this weighted collection efficiency is more meaningful because the number of elementary charges a particle carries is usually an integer. Moreover, the collection efficiency is generally a nonlinear function of the number of charges, and then, there might be some difference between these two calculation methods.

4. Simulation Results and Discussion

The parameters and constants used in this work are listed in Table 1, if not otherwise specified. The models for the charging and collecting stages, as presented in the previous sections, are solved numerically using Matlab, and the main results are highlighted below.

Figure 2 shows the first eight combination coefficients (β_0−β_7) of particles with positive ions based on the Fuchs' theory. It is seen from this figure that the combination coefficient decreases sharply as the particle acquires more and more ions. For particles having the same number of elementary charges, the larger the particle size, the larger the combination coefficient. Also, it can be seen from this figure that only β_0 is of importance for particles with size less than 10 nm, which is consistent with the experimental observation that particles in the ultrafine size range rarely acquire more than one unit of charge.[6]

To demonstrate the unipolar charging behavior of particles in the charging process, the charge distribution as a function of the product of ion concentration and charging time, for two particles of two different diameters, 20 nm (dashed lines) and 50 nm (solid lines) is shown in Figure 3. Figure 3 indicates that the charging fraction is not uniformly distributed for particles in the nanosize range, as a result of the dynamic interplay of different combination coefficients. Because $-\beta_0 < -\beta_1 < ... < -\beta_{p-1} < 0$, there is typically a peak in the charging

Table 1. Parameters Used in the Process Model

temperature (K)	292
particle diameter, d_p (nm)	5−100
mean thermal mobility of positive ions, C_{ion} (m^2/V·s)	1.4×10^{-4}
specific dielectric constant of NaCl aerosols, κ	6.12
ion concentration, n_{ion} (s/m^3)	8.0×10^{13}
molecular weight of positive ion, M_{ion} (kg/mol)	0.109
molecular weight of air, M_{air} (kg/mol)	2.89×10^{-2}
mean free path of air, λ_{air} (m)	6.5×10^{-8}
Avogadro's number N_a (1/mol)	6.0238×10^{23}
elementary electrostatic charge, e (C)	1.6021×10^{-19}
dielectric constant, ϵ_0 (F/m)	8.855×10^{-12}
Boltzman constant, k (J/K)	1.3806×10^{-23}
viscosity of air, μ (kg/m·s)	18.1×10^{-6}
kinetic viscosity of air, ν (m^2/s)	1.506×10^{-5}
length of collecting cell, L (m)	0.197
half width of collecting cell, R (m)	5.9×10^{-3}
particle mean velocity, u_0 (m/s)	3.0
electrostatic intensity (10^3 V/cm)	5.0

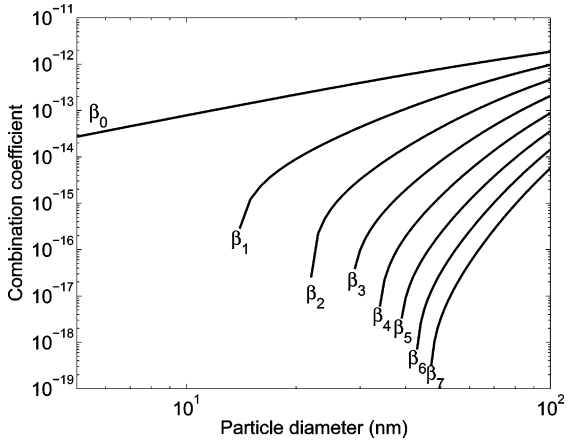

Figure 2. Combination coefficients of NaCl nanosize particles with positive ions.

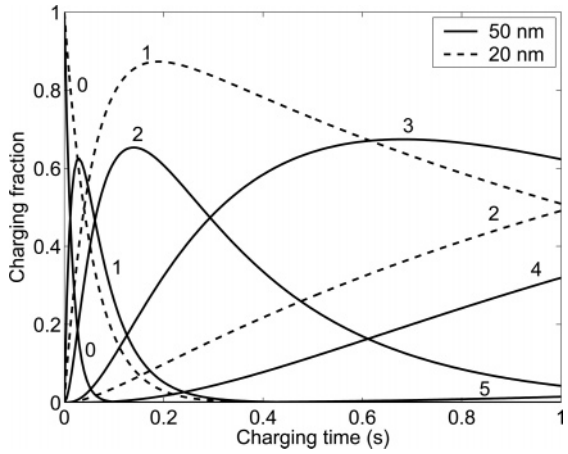

Figure 3. Charging fraction as a function of charging time ($n_{ion} = 8 \times 10^{13}$/m^3) for two different particle sizes (dashed curves, $d_p = 20$ nm, and solid curves, $d_p = 50$ nm).

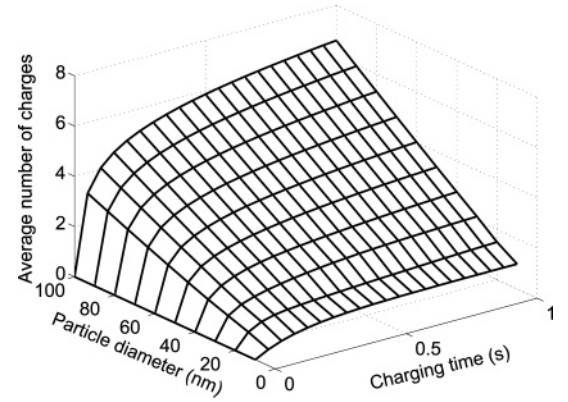

Figure 4. Average number of charges as a function of particle diameter and the product of ion concentration and charging time ($n_{ion} = 8 \times 10^{13}$/m^3).

fraction $f_1 - f_{p-1}$, while f_0 is continuously decreasing and f_p is steadily increasing. However, the average number of elementary charges the particles acquire is always increasing as $n_{ion}t$ increases, as shown in Figure 4. It is also seen that the number of charges that nanosize particles acquire is quite limited. When $n_{ion}t = 8 \times 10^{13}$ s/m^3, particles of size 10 nm acquire an average number of 0.998 (less than 1) unit of charge, while particles of size 100 nm acquire an average number of 6.296 units of charge. Under the same value of $n_{ion}t$, the average number of charges the particles carry is nearly a linear function of particle size. For example, when $n_{ion}t = 8 \times 10^{13}$ s/m^3, the relationship can be expressed by $0.059 \times (d_p/1\text{ nm}) + 0.371$. Also shown in Table 2 is the charging fraction of particles of different sizes as a function of $n_{ion}t$ and a comparison with experimental data[6] in terms of the overall charged fraction. This comparison indicates that the Fuchs' theory might overestimate β_0 for particles in the nanosize range. The deviation becomes smaller as d_p or $n_{ion}t$ becomes larger.

Table 2. Charged Fraction as a Function of Particle Size and $n_{ion}t$, Predicted by Model and Experiments[6]

d_p (nm)	f_0	f_1	f_2	f_3	f_4	f_5	f_c^{calc}	f_c^{exp}	dev.
				(a) $n_{ion}t = 2.75 \times 10^{12}$ s/m^3					
13	0.726	0.274					0.274	0.233	18%
18	0.595	0.402	0.003				0.405	0.303	34%
24	0.454	0.530	0.016				0.546	0.436	25%
32	0.305	0.637	0.058				0.695	0.567	23%
42	0.178	0.663	0.156	0.003			0.822	0.683	20%
56	0.081	0.558	0.334	0.027			0.919	0.890	3%
75	0.027	0.338	0.496	0.132	0.008		0.973	0.912	7%
				(b) $n_{ion}t = 6.68 \times 10^{12}$ s/m^3					
13	0.460	0.541					0.541	0.400	35%
18	0.283	0.702	0.015				0.717	0.547	31%
24	0.147	0.784	0.069				0.853	0.711	20%
32	0.056	0.733	0.209	0.003			0.944	0.834	13%
42	0.015	0.522	0.436	0.027			0.985	0.923	7%
56	0.002	0.227	0.607	0.158	0.006		0.998	0.976	2%
75		0.045	0.427	0.444	0.081	0.003	1.000	0.995	0%
				(c) $n_{ion}t = 9.53 \times 10^{12}$ s/m^3					
13	0.330	0.670					0.670	0.502	34%
18	0.166	0.808	0.026				0.835	0.665	25%
24	0.065	0.822	0.113				0.935	0.803	16%
32	0.016	0.664	0.313	0.006			0.984	0.916	7%
42	0.003	0.376	0.566	0.055	0.001		0.998	0.969	3%
56		0.106	0.611	0.269	0.015		1.000	0.994	1%
75		0.010	0.270	0.543	0.167	0.010	1.000		

Figure 5 demonstrates a typical concentration profile of particles in the electrostatic field. Upon entering the charging stage, the particle concentration is uniformly n_0, although the charging fraction is nonuniform (even for monodisperse particles). As the suspended particles with the carrier air pass through the electrostatic precipitator, the particles migrate to the grounded collection plates because of the electrostatic force and the particle concentration drops near the collection plate. However, it is seen that the maximum particle concentration is not on the symmetric surface but somewhere between this surface and the collecting plates. This is because there is no accumulation of particles at the symmetric surface $y = 0$ where the mass flux due to the negative concentration gradient cancels the migration rate.

Figure 6 demonstrates the single collection efficiency as a function of the particle size and the number of elementary

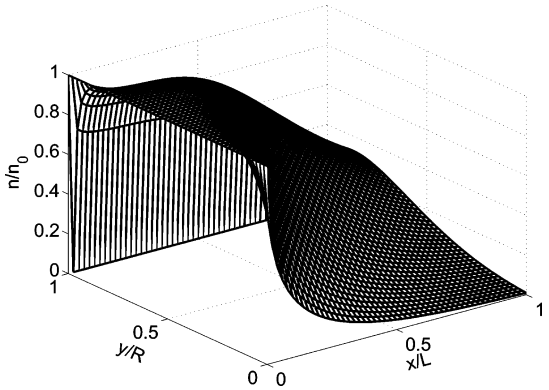

Figure 5. Typical particle concentration profile in the electrostatic precipitator ($d_p = 50$ nm, $i = 2$).

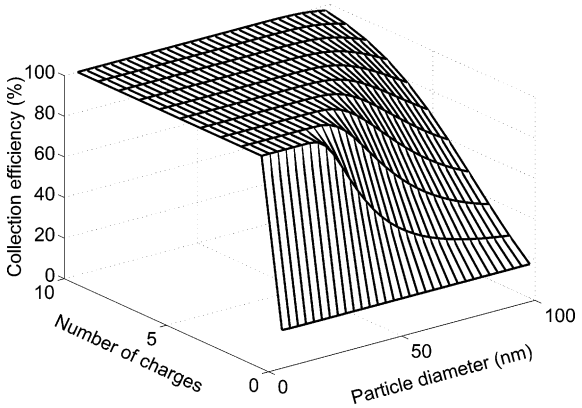

Figure 6. Single collection efficiency as a function of particle size (5−100 nm) and number of elementary charges.

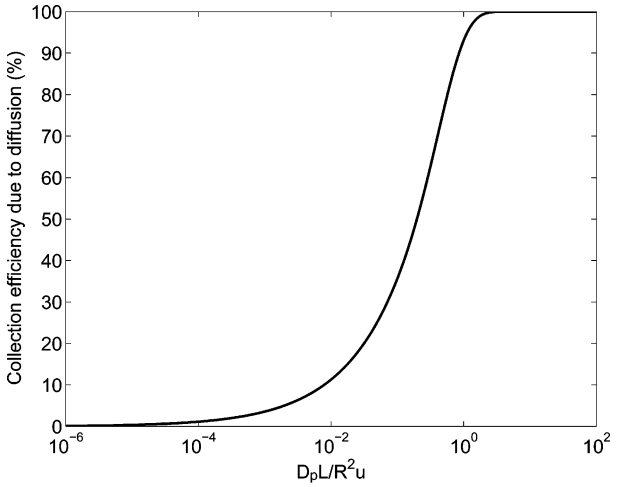

Figure 7. Theoretical prediction of collection efficiency due to constant diffusion.

charges. It is obvious that ultrafine particles tend to be removed by the electrostatic precipitator much more easily than larger ones if they carry the same number of elementary charges, which can be explained by the higher migration velocity of smaller particles under the same electrostatic force. Moreover, under the current simulation settings, the collection efficiency for ultrafine particles is almost the same (close to unity) as long as they are charged, no matter how many units of charge they carry (although they seldom carry more than one unit of charge). For larger particles, however, the collection efficiency is dependent on the number of charges they acquire. Furthermore, the larger the number of charges, the higher the collection efficiency. For uncharged particles, some of them might also be collected on the grounded plate as a result of diffusion. Generally speaking, the collection efficiency of nanosize particles due to diffusion is a weak function of particle size, and it is relatively small as compared to the one due to electrostatic precipitation, as shown in Figure 6. In fact, under the assumption of constant dispersion, an analytic expression for the collection efficiency can be derived as

$$\eta = 1 - \frac{8}{\pi^2}\sum_{i=1}^{\infty}\frac{1}{(2i-1)^2}\exp\left[-\frac{(2i-1)^2\pi^2 D_p}{4R^2u}L\right]$$

(see the appendix for details). Theoretical collection efficiency due to constant diffusion is shown in Figure 7 as a function of D_pL/R^2U, which is typically small because D_pL/R^2U is on the order of 10^{-2} or even smaller.

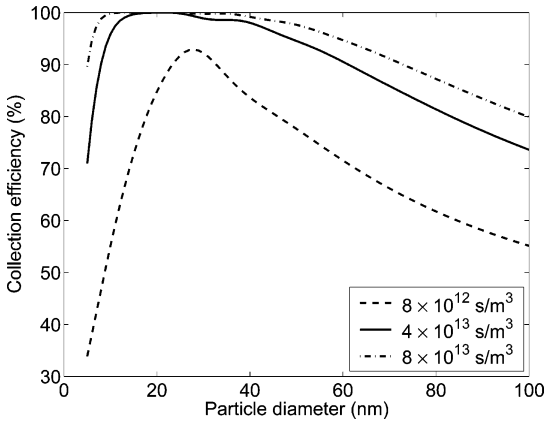

Figure 8. Overall collection efficiency as a function of $n_{ion}t$ and particle size.

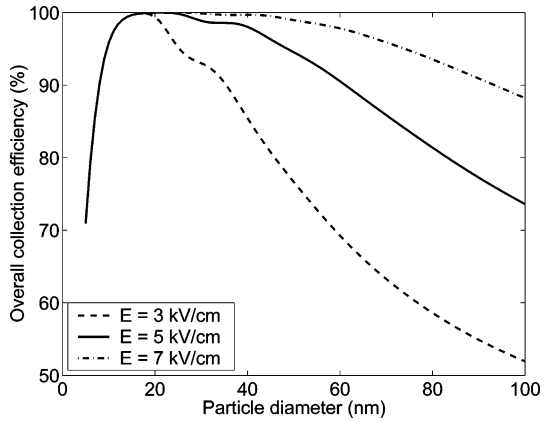

Figure 9. Overall collection efficiency as a function of electrostatic intensity and particle diameter ($n_{ion}t = 4 \times 10^{13}$ s/m^3).

Figure 8 shows the relationship between the overall collection efficiency and the particle diameter for three $n_{ion}t$ levels (8×10^{12} s/m^3, 4×10^{12} s/m^3, and 8×10^{13} s/m^3). It can be seen that under the same $n_{ion}t$ product, the overall collection efficiency usually goes up first, reaching a peak, and then decreases as the particle diameter increases from 5 nm to 100 nm. This phenomenon results from the interplay of the increasing charging fraction (refer to Figure 4) and the decreasing electrostatic mobility (refer to Figure 6). Because particles in the ultrafine size range usually have very high electrostatic migration velocity, the overall collection efficiency is close to unity when $n_{ion}t$ is large enough and the particles are almost fully charged by acquiring one ion. However, as $n_{ion}t$ decreases, the collection efficiency for very small particles drops significantly (because of decreased charging fraction) and the peak in the collection efficiency shifts to the right.

Figure 9 demonstrates the overall collection efficiency as a function of particle diameter and the electrostatic intensity. It can be seen from this figure that an increase in the electrostatic intensity usually results in an increase in the overall collection efficiency because the migration velocity increases. But for particles in the ultrafine size range, the electrostatic intensity has almost no effect on the overall collection efficiency. This is because the collection efficiency for these particles is almost 100% if they acquire just one unit of charge (or the collection is limited by the charging fraction), and a further increase in the electrostatic migration velocity due to enhanced electrostatic intensity does not improve the collection efficiency.

The peak in the collection efficiency of nanoparticles as a function of particle size was reported by experimental work in the literature. For example, in the work of Yoo et al.,[38] the

maximum of the collection efficiency for nanosize NaCl particles in the nanosize range occurred around $d_p = 40-50$ nm in a two-stage electrostatic precipitator under the experimental settings of interest and was explained by the partial charging effect for $d_p \leq 30\ \mu$m. In the work of Zhuang et al.,[25] the peak occurred between 60 nm and 80 nm for silica particles, under two different voltages in the collection stage. It was also shown that, under higher voltage, the collection efficiency increased for coarse particles (larger than about 60 nm) only and retained almost the same value for finer particles (smaller than about 60 nm). Moreover, the peak shifted to the right when the voltage in the collection stage increased. These phenomena are consistent with the model predictions in the current work and can be explained accordingly.

5. Concluding Remarks

The collection efficiency for particles in the nanosize range (5−100 nm) in a two-stage parallel electrostatic precipitator is studied by numerical simulation in this paper. The charging process is based on the theories of Fuchs. For the collecting stage, the mass transfer model includes Brownian and eddy diffusion, turbulent flow, and migration. Calculation results indicate the following:

(1) The particle charging fraction is not uniformly distributed in the nanosize range. Ultrafine particles with diameter less than 20 nm seldom acquire more than one unit of charge. Large particles with diameter larger than 20 nm might acquire several units of charge, depending on the product of ion concentration and charging time.

(2) The average number of charges a particle acquires increases with the particle size and the product of ion concentration and charging time. Particles in the size range between 5 and 100 nm can seldom capture more than 10 units of charge if the product of ion concentration and charging time is less than 8×10^{13} s/cm^3.

(3) There is usually a peak in the particle size and collection efficiency profile, which is caused by the higher electrostatic mobility of the ultrafine particles and the higher charging probabilities of the coarser particles. This peak might vary depending on the parameters in the charging and collecting stages. Similar experimental observations have been reported in the literature.

(4) Particles with diameter less than 20 nm have more electrostatic mobility than bigger ones. Therefore, the most efficient way to increase their collection efficiency is to increase the product of charging time and ion concentration. For particles with larger size, both the parameters in the charging stage (the product of ion concentration and charging time) and those in the collection stage (electrostatic intensity, length, and width) may have an important effect on the collection efficiency.

Acknowledgment

Financial support from a 2001 Office of Naval Research Young Investigator Award, program manager Dr. Lawrence Kabacoff, is gratefully acknowledged.

Appendix: Analytic Solution to Collection Efficiency for Particles Due to Constant Diffusion

The partial differential equation (PDE) that describes the transport phenomena in an electrostatic precipitator with constant dispersion and no electrostatic migration is given by

$$u\frac{\partial n}{\partial x} = D_p\frac{\partial^2 n}{\partial y^2} \tag{18}$$

subject to the boundary conditions

$$n = n_0, \quad \forall y, \quad x = 0$$

$$n = 0, \quad \forall x, \quad y = 0$$

$$-D_p\frac{\partial n}{\partial y} = 0, \quad \forall x, \quad y = R \tag{19}$$

When Laplace transformation is used, the above PDE can be converted into an ordinary differential equation of the form

$$u(s\bar{n} - n_0) = D_p\frac{\partial^2 \bar{n}}{\partial y^2}$$

s.t.

$$\bar{n} = 0, \quad \forall x, \quad y = 0$$

$$-D_p\frac{\partial \bar{n}}{\partial y} = 0, \quad \forall x, \quad y = R \tag{20}$$

whose solution is of the following form

$$\bar{n} = \frac{n_0}{s} - \frac{n_0}{s}\frac{\cosh\left(\sqrt{\frac{us}{D_p}}y\right)}{\cosh\left(\sqrt{\frac{us}{D_p}}R\right)} \tag{21}$$

By referring to standard Laplace transformation tables,[39] the following is found:

$$L^{-1}\left[\frac{\cosh(z\sqrt{s})}{s\cosh(a\sqrt{s})}\right] = 1 + \frac{4}{\pi}\sum_{n=1}^{\infty}\frac{(-1)^n}{2n-1}\exp\left[-\frac{(2n-1)^2\pi^2}{4a^2}x\right]\cos\left[\frac{(2n-1)\pi z}{2a}\right] \tag{22}$$

and, thus, eq 22 yields

$$n(x, y) = n_0\left\{\frac{4}{\pi}\sum_{i=1}^{\infty}\frac{(-1)^{i+1}}{2i-1}\exp\left[-\frac{(2i-1)^2\pi^2 D_p}{4R^2 u}x\right]\cos\left[\frac{(2i-1)\pi y}{2R}\right]\right\} \tag{23}$$

The average concentration at the outlet of the container can be computed by

$$n_{ave}(L) = \frac{1}{R}\int_0^R n_{x=L}\,dy = n_0\left\{\frac{8}{\pi^2}\sum_{i=1}^{\infty}\frac{1}{(2i-1)^2}\exp\left[-\frac{(2i-1)^2\pi^2 D_p}{4R^2 u}L\right]\right\} \tag{24}$$

Therefore, the analytic expression to calculate the collection efficiency for particles without charge is

$$\eta = 1 - \frac{n_{ave}}{n_0} = 1 - \frac{8}{\pi^2}\sum_{i=1}^{\infty}\frac{1}{(2i-1)^2}\exp\left[-\frac{(2i-1)^2\pi^2 D_p}{4R^2 u}L\right] \quad (25)$$

Literature Cited

(1) Friedlander, S. K. *Smoke, Dust and Haze: Fundamentals of Aerosol Dynamics*, 2nd ed.; Oxford University Press: New York, 2000.

(2) Kruis, F. E.; Goossens, A.; Fissan, H. Synthesis of semiconducting nanoparticles. *J. Aerosol Sci.* **1996**, *27*, S165−S166.

(3) Karthikeyan, J.; Berndt, C. C.; Tikkanen, J.; Reddy, S.; Herman, H. Plasma spray synthesis of nanomaterial powders and deposits. *Mater. Sci. Eng., A* **1997**, *238*, 275−286.

(4) Karthikeyan, J.; Berndt, C. C.; Tikkanen, J.; Wang, J. Y.; King, A. H.; Herman, H. Nanomaterial powders and deposits prepared by flame spray processing of liquid precursors. *Nanostruct. Mater.* **1997**, *8*, 61−74.

(5) Koizumi, Y.; Kawamura, M.; Tochikubo, F.; Watanabe, T. Estimation of the agglomeration coefficient of bipolar-charged aerosol particles. *J. Electrostatics* **2000**, *48*, 93−101.

(6) Pui, D. Y. H.; Fruin, S.; McMurry, P. H. Unipolar diffusion charging of ultrafine aerosols. *Aerosol Sci. Technol.* **1988**, *8*, 173−187.

(7) Leonard, G.; Mitchner, M.; Self, S. A. Particle transport in electrostatic precipitators. *Atmos. Environ.* **1980**, *14*, 1289−1299.

(8) Hassid, S.; Oron, A.; Gutfinger, C. An asymptotic description of electrostatic precipitation of charged particles in turbulent flow. *J. Aerosol Sci.* **1987**, *18*, 357−367.

(9) Oron, A.; Gutfinger, C.; Hassid, S. Turbulent deposition of charged particles under the influence of an external electric field. *J. Colloid Interface Sci.* **1988**, *121*, 531−542.

(10) Park, J.; Chun, C. An improved modelling for prediction of grade efficiency of electrostatic precipitators with negative corona. *J. Aerosol Sci.* **2002**, *33*, 673−694.

(11) Kallio, G. A.; Reeks, M. W. A numerical simulation of particle deposition in turbulent boundary layers. *Int. J. Multiphase Flow* **1989**, *15*, 433−446.

(12) Goo, J. H.; Lee, J. W. Monte-carlo simulation of turbulent deposition of charged particles in a plate-plate electrostatic precipitator. *Aerosol Sci. Technol.* **1996**, *25*, 31−45.

(13) Choi, B. S.; Fletcher, C. A. J. Turbulent particle dispersion in an electrostatic precipitator. *Applied Mathematical Modelling* **1998**, *22*, 1009−1021.

(14) Soldati, A.; Casal, M.; Andreussi, P.; Banerjee, S. Lagrangian simulation of turbulent particle dispersion in electrostatic precipitators. *AIChE J.* **1997**, *43*, 1403−1413.

(15) Soldati, A. On the effects of electrohydrodynamic flows and turbulence on aerosol transport and collection in wire-plate electrostatic precipitators. *J. Aerosol Sci.* **2000**, *31*, 293−305.

(16) Goo, J. H.; Lee, J. W. Stochastic simulation of particle charging and collection characteristics for a wire-plate electrostatic precipitator of short length. *J. Aerosol Sci.* **1997**, *28*, 875−893.

(17) Kim, S. H.; Park, H. S.; Lee, K. W. Theoretical model of electrostatic precipitator performance for collecting polydisperse particles. *J. Electrost.* **2001**, *50*, 177−190.

(18) Park, H. S.; Jung, C. H.; Lee, K. W. Analytic solution for collection efficiency of electrostatic precipitators for polydisperse aerosols. *Environ. Eng. Sci.* **2004**, *21*, 451−461.

(19) Varonos, A. A.; Anagnostopoulos, J. S.; Bergeles, G. C. Prediction of the cleaning efficiency of an electrostatic precipitator. *J. Electrostatics* **2002**, *55*, 111−133.

(20) Yeh, H. C. Electrical Techniques. In *Aerosol Measurement*; Willeke, K., Baron, P. A., Eds.; Van Nostrand Reinhold: New York, 1993.

(21) Marlow, W. H.; Brock, J. R. Unipolar charging of small aerosol particles. *J. Colloid Interface Sci.* **1975**, *50*, 32−38.

(22) Fuchs, N. A. On the stationary charge distribution on aerosol particles in a bipolar ionic atmosphere. *Geofis. Pura Appl.* **1963**, *56*, 185−193.

(23) Boisdron, Y.; Brock, J. R. On the stochastic nature of the acquisition of electrical charge and radioactivity by aerosol particles. *Atmos. Environ.* **1970**, *4*, 35−50.

(24) Adachi, M.; Kousaka, Y.; Okuyama, K. Unipolar and bipolar diffusion charging of ultrafine aerosol particles. *J. Aerosol Sci.* **1985**, *16*, 109−123.

(25) Zhuang, Y.; Kim, Y. J.; Lee, T. G.; Biswas, P. Experimental and Theoretical Studies of Ultra-fine Particle Behavior in Electrostatic Precipitators. *J. Electrost.* **2000**, *48*, 245−260.

(26) Kailath, T. *Linear Systems*; Prentice Hall: Englewood Cliffs, NJ, 1980.

(27) Talaie, M. R. Mathematical modeling of wire-duct single-stage electrostatic precipitators. *J. Hazard. Mater.* **2005**, *124*, 44−52.

(28) Park, S. J.; Kim, S. S. Effects of particle space charge and turbulent diffusion on performance of plate-plate electrostatic precipitators. *J. Electrost.* **1998**, *45*, 121−137.

(29) Talaie, M. R.; Fathikaljahi, J.; Taheri, M.; Bahri, P. Mathematical modeling of double-stage electrostatic precipitators based on a modified Eulerian approach. *Aerosol Sci. Technol.* **2001**, *34*, 512−519.

(30) Li, M.; Christofides, P. D. Multi-scale modeling and analysis of HVOF thermal spray process. *Chem. Eng. Sci.* **2005**, *60*, 3649−3669.

(31) Li, M.; Shi, D.; Christofides, P. D. Diamond Jet Hybrid HVOF Thermal Spray: Gas-Phase and Particle Behavior Modeling and Feedback Control Design. *Ind. Eng. Chem. Res.* **2004**, *43*, 3632−3652.

(32) Shi, D.; Li, M.; Christofides, P. D. Diamond Jet Hybrid HVOF Thermal Spray: Rule-Based Modeling of Coating Microstructure. *Ind. Eng. Chem. Res.* **2004**, *43*, 3653−3665.

(33) Kalani, A.; Christofides, P. D. Modeling and control of a titania aerosol reactor. *Aerosol Sci. Technol.* **2000**, *32*, 369−391.

(34) Chiu, T.; Christofides, P. D. Nonlinear control of particulate processes. *AIChE J.* **1999**, *45*, 1279−1297.

(35) Christofides, P. D. *Model-Based Control of Particulate Processes*; Particle Technology Series; Kluwer Academic Publishers: Amsterdam, The Netherlands, 2002.

(36) Kihm, K. D.; Mitchner, M.; Self, S. A. Comparison of wire-plate and plate-plate electrostatic precipitators in turbulent flow. *J. Electrost.* **1987**, *19*, 21−32.

(37) Hinze, J. O. *Turbulence*; McGraw-Hill: New York, 1975.

(38) Yoo, K. H.; Lee, J. S.; Oh, M. D. Charging and collection of submicron particles in two-stage parallel-plate electrostatic precipitators. *Aerosol Sci. Technol.* **1997**, *27*, 308−323.

(39) Spiegel, M. R. *Mathematical Handbook of Formulas and Tables*; McGraw-Hill: New York, 1968.

Received for review January 22, 2006
Revised manuscript received March 13, 2006
Accepted March 17, 2006

IE060101R